Journal of Materials Chemistry B

ROYAL SOCIETY OF CHEMISTRY

PAPER

View Article Online
View Journal | View Issue

Cite this: J. Mater. Chem. B, 2024, 12, 12017

Nanoassemblies with Gd-chelating lipids (GMO@DTPA-BSA-Gd) as a potential new type of high molecular weight contrast agents†

Karolina Dydak, [ab] Tomasz Zalewski, [b] Marek Kempka,[ab] Patryk Florczak, [b] Grzegorz Nowaczyk, [b] Łucja Przysiecka, [b] Jakub Jagielski, [b] Benoit Loppinet, [c] Michał Banaszak[ab] and Dorota Flak *[b]

Self-assembled lipid nanoparticles containing Gd-chelating lipids are a new type of positive magnetic resonance imaging contrast agents (MRI CAs). High molecular weight imposes reduced molecular reorientation (τ_r) and corresponding longer reorientation correlation times (τ_c), finally resulting in overall high relaxivity (r_1) of such contrast agents. Therefore, we report nanoassemblies based on two types of amphiphile molecules: glyceryl monooleate (GMO) as a matrix embedded with DTPA-bis(stearylamide) and its gadolinium salt (DTPA-BSA-Gd) as a Gd-chelating lipid, stabilized by surfactant Pluronic F127 molecules. The loading of DTPA-BSA-Gd into the GMO matrix was investigated at low (5% w/w) and high (30, 40, 50% w/w) contents. Small angle X-ray scattering (SAXS), cryogenic transmission electron microscopy (cryo-TEM) and dynamic light scattering (DLS) results show that although the nanoassembly of both amphiphile molecules within the nanoparticle is disturbed in terms of the formed phases, this composition ensures their colloidal stability. In nanoparticles with low DTPA-BSA-Gd contents, the assembly results in a cubic diamond phase that is co-existing with a fraction of liposomes. For high DTPA-BSA-Gd contents, swelling of the structure occurs such that the initially formed primitive cubic phase transforms toward a lamellar phase in the nanoassemblies. Results from inductively coupled plasma mass spectrometry (ICP-MS) indicate that for almost all systems, the loading efficiency (LE) of DTPA-BSA-Gd is high (reaching up to approx. 85%), and the nanoassembly provides strong entrapment of Gd^{3+} ions, which are then efficiently uptaken by cells. Moreover, the higher the surfactant content, the higher the LE. The viability studies demonstrate that the prepared nanoassemblies preserve high biocompatibility towards both cancer (HeLa) and normal cells (MSU 1.1). Nuclear magnetic resonance relaxometry studies (NMR relaxometry) followed by MRI on the prepared nanoassembly dispersions proved that the formation of GMO@DTPA-BSA-Gd nanoassemblies, considered as high molecular weight CAs, results in high relaxivity parameters (*e.g.*, r_1 = 19.72 mM^{-1} s^{-1} for 2GMO-40DTPA-10F127) that are superior to commercially developed ones (*e.g.*, Magnevist or Gadovist). These comprehensive studies imply that a high degree of internal ordering of nanoassemblies with a higher content of Gd-chelating lipid is not a decisive factor in determining the increase in relaxivity, thus confirming their potential as positive MRI CAs.

Received 31st July 2024,
Accepted 8th October 2024

DOI: 10.1039/d4tb01684j

rsc.li/materials-b

1. Introduction

MRI is a powerful tool not only for the diagnosis and management of a variety of diseases and treatment monitoring but also for all types of neurological studies. It is a non-invasive technique routinely used in clinics due to its intrinsic spatial resolution and deep tissue penetration and the three-dimensional anatomical information it provides.[1] However, MRI inherently suffers from low sensitivity; hence, the interest in contrast-enhanced MRI has been remarkable since the approval of Gd-DTPA (Magnevist) as an exogenous contrast

[a] Faculty of Physics, Adam Mickiewicz University, Uniwersytetu Poznańskiego 2, 61-614 Poznań, Poland
[b] NanoBioMedical Centre, Adam Mickiewicz University, Wszechnicy Piastowskiej 3, 61-614 Poznań, Poland. E-mail: dorfla@amu.edu.pl; Tel: +48 618296713
[c] Institute of Electronic Structure and Laser, Foundation for Research and Technology-Hellas, P.O. Box 1385, 711 10 Heraklion, Crete, Greece

† Electronic supplementary information (ESI) available. See DOI: https://doi.org/10.1039/d4tb01684j

agent (CA) in 1988.[2] The MRI signal depends on proton density and their relaxation rates, which are largely dependent on the chemical environments. Hence, CAs' role is their effect on the relaxation times of water protons (bulk water molecules). Further, the relaxation rates are characterized by the longitudinal relaxation time (T_1), resultant of the energy exchange between spins and lattice, and by the transverse relaxation time (T_2), resultant of the energy exchange between spins. Accordingly, CAs are divided into positive and negative types that brighten or darken their immediate surrounding area in the image, respectively.[3] There is a great demand for new types of MRI CAs that will substitute the CAs that have been used so far based either on paramagnetic complexes or magnetic nanoparticles.[1] These paramagnetic CAs are gadolinium (Gd^{3+}) or manganese (Mn^{2+}) chelates, shortening the longitudinal relaxation time (T_1) and thus accelerating the longitudinal relaxation (R_1) of water protons and providing a positive (T_1-weighted bright image) contrast in regions of interest, where these CAs localize.[4] Gd-based positive CAs are the gold standard in clinical MRI; however, significant efforts are still taken to design and develop novel Gd-based CAs.[5] Among them are macrocyclic Gd-chelate formulations such as Dotarem (Gd-DOTA, gadoterate) or Gadovist (Gd-DO3A-butrol, gadopentetate dimeglumine), and linear types such as Magnevist (Gd-DTPA, gadopentetate dimeglumine), Multihance (Gd-BOPTA, gadobenate dimeglumine), or Omniscan (Gd-DTPA-BMA, gadodiamide). Alternative to commercial Gd-based CAs was a Teslascan containing Mn^{2+} ions (mangafodipir trisodium). However, Gd-based CAs suffer from possible toxicity and long-term accumulation in brain tissues but also may induce nephrogenic systemic fibrosis (NSF) and resultant renal impairment. Teslascan was initially approved by the Food and Drug Administration (FDA) and EMA only for the detection of lesions in the liver, and the excess of Mn is known to induce cytotoxicity manifested as the abnormal redox potential and changes in the central nervous system. In 2012, based on the decision of the marketing authorization holder, the EMA issued a decision to withdraw the marketing authorization for Teslascan for commercial reasons. Further, in 2017, the EMA recommended restricting the use of some linear gadolinium agents in MRI body scans, suspended the authorizations of others, and maintained only the use of macrocyclic Gd-based chelate formulations. The conclusion is, therefore, that adverse cytotoxic effects of these paramagnetic ions and their accumulation ability in organs cannot be, unfortunately, balanced with their MR imaging efficiency.

Regarding CAs based on magnetic nanoparticles, two types of iron oxide CAs exist: superparamagnetic iron oxide (SPIO) and ultrasmall superparamagnetic iron oxide (USPIO).[6] These nanoparticles have emerged as prevailing negative (T_2-weighted dark image) CAs due to enhancing the transverse relaxivity (r_2) by shortening the transverse relaxation time (T_2 and T_2*). SPIO and USPIO CAs have been used successfully in some instances for liver lesions and tropism, ganglion tropism evaluation or diagnosis of a variety of central nervous system diseases. However, the negative contrast they provide and magnetic susceptibility artefacts hamper their use in MRI, as they can mislead the image-based diagnosis. Moreover, production and thus the use of CAs based on ferrite nanoparticles, such as Sinerem, Resovist, Feridex or others, was either discontinued or the marketing authorization application was withdrawn.

Therefore, to overcome the above-mentioned drawbacks of CAs types used so far, the challenge is to obtain a new type of CAs exhibiting positive contrast ability, with an increased relaxivity r_1, and with ensured physico-chemical stability and high biocompatibility. For high intracellular uptake and accumulation, the best cell-type specific and favorable pharmacokinetics and pharmacodynamics should be considered, resulting in minimal side effects to an organism.

Gadolinium chelates, so far, are the leading type of MRI CAs, and despite great scientific and research efforts, it seems that Gd cannot be entirely excluded from that research.[5] The promising direction is the design of high molecular weight Gd ion-containing CAs, which exhibit reduced molecular reorientation (τ_r) with correspondingly longer reorientation correlation times (τ_c), resulting in high relaxivity.[3] On the other hand, it can ensure the physico-chemical stability of the system and limits the Gd^{3+} ion leakage, hence reducing its toxicity. This can be achieved by increasing the molecular weight of the CA by increasing the molecular weight of the Gd-containing complex or by combining (embedding) Gd-containing complexes into a macromolecule (*e.g.*, biological molecules, polymers, dendrimers) or in nanoparticles of different types (*e.g.*, polymeric, inorganic, hybrids). For example, Yang *et al.*[7] showed that increasing the molecular weight of CA through engineered proteins (Mw ~ 12 kDa) chelated with Gd^{3+} improved the relaxivities 20 times in comparison to that of Gd-DTPA. Mi *et al.*[8] presented the positive effect of confining Gd-DTPA inside the core of the polymeric micelles, resulting in a relaxivity increase of more than 13 times as compared with that of Gd-DTPA itself.

In this work, we propose to use both approaches, namely embedding Gd-chelating lipids (DTPA-BSA-Gd, (diethylenetriaminepentaacetic acid)-bis(stearylamide) (gadolinium salt)) of increased molecular weight in comparison to Gd-chelates (Gd-DTPA, gadopentetic acid) into GMO-based lipid nanoparticles (glycerol monooleate). It is expected, that in this way, they will form supramolecular structures by the self-assembly process of both amphiphilic molecules of DTPA-BSA-Gd and GMO matrix molecules (GMO@DTPA-BSA-Gd). GMO is one of the most common lipids used for the formation of, *e.g.*, lyotropic liquid crystalline nanoparticles (LLCNPs) as drug carriers. It has been approved by the FDA and is considered biocompatible. Moreover, lipid-based nanoparticles show the tendency to passively accumulate in tumor tissues due to the enhanced permeability and retention effect (EPR), which eventually provides a higher signal-to-noise ratio in tumors during MR imaging. Another observed advantage is that lipid nanoassemblies with DTPA-BSA-Gd exhibit prolonged blood circulation and improved physico-chemical stability when studied *in vivo*, ensuring the longevity of the MRI contrast.[9] Gd-chelated lipids as CAs have already been used in the modification of various types of nanoparticles, including lipid ones.[9–11] However, GMO-based systems modified with Gd-chelating lipids have not been fully investigated so far. Further, the advantages of the proposed

lipid-based nanoparticles allow us to conclude that the proposed (Gd)-chelating lipid-enriched GMO-lipid nanoparticles represent a promising class of contrast agents for magnetic resonance MR imaging. Moreover, these nanocarriers offer significant potential for the development of multifunctional systems that integrate diagnostic and therapeutic capabilities within a single platform. Notably, Flak *et al.*[12] successfully employed cubosomes as carriers for the AT101 drug in glioblastoma multiforme therapy, wherein the incorporation of the drug into the nanoparticle matrix enhanced its solubility in aqueous environments and significantly improved its previously limited biocompatibility.

Therefore, this study aimed to investigate self-assembled amphiphile systems as carriers for paramagnetic metals in the form of Gd-chelating lipid (DTPA-BSA-Gd) and its potential in MR imaging. The possibility of incorporating DTPA-BSA-Gd into the GMO matrix at different content levels (low and high), its impact on the type of formed structure, their relaxometric performance, and finally, MRI contrasting efficiency are presented. Further, the DTPA-BSA-Gd loading efficiency into the GMO matrix was investigated, and finally, the cell uptake. This study also provides evidence of the biocompatibility of the prepared nanoassemblies *in vitro*.

2. Experimental/materials and methods

2.1. Preparation of GMO@DTPA-BSA-Gd nanoassemblies

In the presented work, the adapted top-down method[13] was used to prepare lipid-based nanoassemblies. The block diagram of the GMO@DTPA-BSA-Gd nanoassembly preparation is given in Fig. 1I. In the first stage, a mixture of the basic structure-forming lipid glyceryl monooleate (GMO; IOI Oleochemicals; M = 356.5 g mol^{-1}) and gadolinium chelating lipid (diethylenetriaminepentaacetic acid)-bis(stearylamide) (gadolinium salt), with double alkyl chain (DTPA-BSA-Gd; Avanti Polar Lipids; M = 1050.56 g mol^{-1}), were prepared by the addition of DTPA-BSA-Gd (0, 5, 30, 40, 50% w/w to GMO, further named as 2GMO, 2GMO-5DTPA, 2GMO-30DTPA, 2GMO-40DTPA, 2GMO-50DTPA) as a solution in a mixture of chloroform and methanol (1 : 1, v/v). The resulting lipid mixture was then homogenized by vortex mixing and vacuum evaporated at 60 °C to remove the organic solvents. Next, the lipid mixture was added with the pre-warmed up to 60 °C aqueous solution of Pluronic F127 surfactant (Sigma-Aldrich; $M \approx$ 12 600 g mol^{-1}) to gain a final concentration of 2% w/w of GMO (20 mg mL^{-1}) and different concentrations of the surfactant (10, 15, 25% w/w to GMO, further named as 2GMO-10F127, 2GMO-15F127, 2GMO-25F127) in an obtained water dispersion. The samples were left for an hour at 60 °C and then for 24 hours at room temperature to obtain a bulk lipid phase. Colloidal nanoparticle dispersions were then formed using high-energy pulsed ultrasonication (Branson Sonifier 250, Emerson Electric Company) at an output power of 40 W. After 24 hours of stabilization at room temperature, samples were purified from the observed unincorporated Gd-DTPA-BSA precipitate by centrifugation (15 min, 10 000 rpm), and the supernatant was collected for further study.[14]

2.2. Characterization of physico-chemical properties

2.2.1. Small angle X-ray scattering (SAXS). SAXS measurements were performed using an Xeus 3.0 setup equipped with a Dectris Eiger 1 M detector. The sample-detector distance was 900 mm. The samples were introduced in a flow cell (Xenocs low noise flow cell) and measured for one hour. Background scattering from water and the cell was subtracted.

2.2.2. Cryogenic transmission electron microscopy (cryo-TEM). The morphology and the structure of prepared nanoassemblies were analyzed using the cryogenic technique (cryo-TEM, Jeol JEM-1400 TEM operating at 120 kV), maintaining a low temperature of about 175 °C during the observation. The prepared nanoparticle dispersions prior to analysis were deposited on previously plasma-treated copper grids covered with Lacey Carbon (Ted Pella Inc.) and freeze-dried at 173 °C with the Cryoplunge 3 System (Gatan Inc.). To verify the structure of the obtained nanoparticles showing internal order, the Fourier transform was used for selected images, and then the reverse transformation was applied to obtain a filtered image.

2.2.3. Dynamic light scattering (DLS) and zeta potential measurements. The particle size and zeta potential of the prepared nanoassemblies, diluted in ultrapure water, were measured on the ZetaSizer Nano ZS (Malvern Panalytical) apparatus, equipped with a 4 mW He–Ne laser (λ = 633 nm), using a non-invasive method of dynamic light scattering with a detection angle of 173° and electrophoretic light scattering. Measurements were carried out at 25 °C using folded capillary cells. Analyzes were performed every 7 days and were terminated after 7 weeks. Each measurement was performed using three individual analyses for each sample, and the results $D_{\text{Intensity}}$, D_{Number}, Z-average, and PdI are given as the mean ± standard deviation (SD).

2.2.4. Inductively coupled plasma mass spectrometry (ICP-MS) – analysis of Gd^{3+} ion content. The analyses were performed on a NexION 5000 apparatus, a four-quadrupole system equipped with tandem mass analyzers (Q1 and Q3) and Universal Cell Technology (UCT). The Syngistix PerkinElmer software was used for data acquisition. Standard ICP-MS analysis was used for the quantification of the total Gd^{3+} ion content in the sample ($[Gd^{3+}]_{\text{FinalSTD}}$). Prior to the analysis, the prepared nanoassembly dispersions (1 mg mL^{-1} of lipid) were mineralized for 48 h with concentrated nitric acid (HNO_3, 65% Suprapur®) to release free Gd^{3+} from the prepared nanoassemblies. Further appropriate dilutions were prepared using ultrapure water (18.2 MΩ × cm, Milli-Q system) and analyses were performed in standard mode using the glass cyclonic spray chamber. A single-elemental standard solution of gadolinium (1 μg mL^{-1}, TruQms, PerkinElmer) was used in appropriate dilutions for obtaining the calibration curve. The obtained results were further used for the relaxometric studies and for calculating the loading efficiency (LE%) of Gd^{3+} ions within nanoassemblies, the result of DTPA-BSA-Gd entrapment.

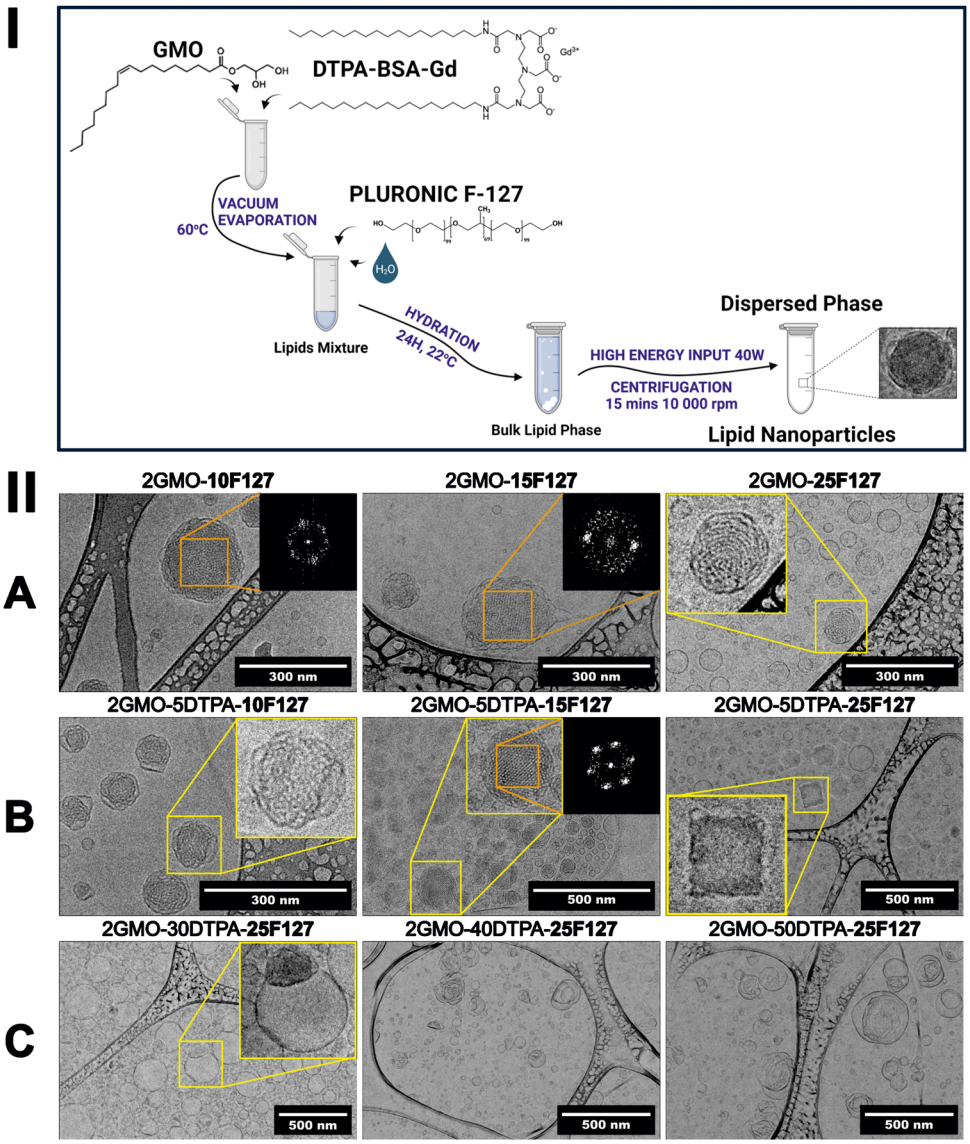

Fig. 1 (I) The block diagram of the GMO@DTPA-BSA-Gd nanoassembly preparation with the top-down method; (II) Cryo-TEM images of prepared nanoassemblies: (A-top row) unmodified system (2GMO-F127) with different surfactant F-127 concentration (10, 15, 25% w/w); (B-middle row) nanoassemblies with low DTPA-BSA-Gd content (5% w/w); (C-bottom row) nanoassemblies with high DTPA-BSA-Gd contents (30, 40, 50% w/w). For selected nanoassembly images, Fast Fourier transformation (in the insets) was applied to show a highly ordered structure.

ICP-MS instrument settings, data acquisition parameters, and calibration data are presented in Table S2 (ESI†).

2.2.5. Nuclear magnetic resonance relaxometry studies-^{1}H NMR relaxometry. Relaxation parameters-the relaxation parameters of prepared nanoassemblies were investigated with NMR longitudinal relaxation time (T_1) measurements performed through the inversion recovery (IR) experiment at a magnetic field of 0.39 T (16.5 MHz) using a home-built spectrometer at room temperature (23 °C). The obtained data showed mono-exponential behavior and were fitted using the function $M(t) = M0^*(1–2\exp(-t/T_1))$. Finally, the dependence of relaxation rate R_1 *vs.* Gd^{3+} concentration was used to calculate the relaxivity parameters r_1. For the measurements, nanoparticle dispersions with different lipid concentrations corresponding to different Gd^{3+} ion concentrations were used.

To study the application of GMO@DTPA-BSA-Gd nanoassemblies as a potential CA, T_1 measurements/NMR studies were performed on cervical cancer cells (HeLa). Briefly, 5×10^5 cells were seeded on plates and incubated overnight. Then, 150 μg mL^{-1} of 2GMO-50DTPA-25F127 nanoassemblies (corresponding to 5.6 μM of Gd^{3+}) were used. As a positive control, the same concentration of Gadovist was used, whereas non-treated cells were used as a negative control. After 24-hour incubation, cells were rinsed in PBS, trypsinized, and fixed in 3.7% formaldehyde. Next, the NMR studies were performed.

Magnetic resonance imaging (MRI)-the potential of prepared GMO@DTPA-BSA-Gd nanoassemblies as MRI contrast agents was examined by a collection of T_1-and T_2-weighted MR images, using a 9.4 Tesla (T) MRI horizontal scanner (Agilent) providing the resonance frequency for protons of 400 MHz,

with the volume RF Millipede coil (30 mm diameter) and 205/120 gradient system. For the experiment, nanoparticle dispersions were appropriately diluted with ultrapure water to obtain final dispersions containing various concentrations of Gd^{3+}, and the ultrapure water sample was used as a reference standard (inserts in Fig. 6III). The values of acquisition parameters of T_1-weighted images acquired with the Multi-Slice Multi Echo – MEMS sequence were set as: repetition time (T_r) – 100 ms; echo time (T_e) – 7.78 ms; averages – 8; field of view (FOV) – 25 × 25 mm; image matrix – 256 × 256; slice thickness – 1 mm. The MEMS imaging sequence with multiple echo registration was used to obtain T_2-weighted images. The sequence was run with the following parameters: T_r – 12 500 ms, T_e – 10 ms, numbers of echoes – 64, averages – 1, FOV – 25 × 25 mm, matrix – 256 × 256, slice thickness – 1 mm.

2.3. Characterization of biological properties

2.3.1. *In vitro* cell culture. The human cervical cancer cell line (HeLa) was sourced from the American Type Culture Collection (ATCC, Virginia, USA). The normal human fibroblast cell line (MSU 1.1) was gratefully provided by Prof. C. Kieda from CBM, CNRS in Orléans, France. Both cell lines were cultured in Dulbecco's Modified Eagle's Medium (DMEM, ThermoFisher Scientific) supplemented with 10% fetal bovine serum (FBS, Gibco Qualified, ThermoFisher Scientific), 100 units per mL penicillin, and 100 μg mL^{-1} streptomycin (ThermoFisher Scientific). Unless specified otherwise, the cells were maintained in a humidified atmosphere with 5% CO_2 at 37 °C.

2.3.2. *In vitro* viability studies. The effect of prepared nanoassemblies on HeLa and MSU 1.1 cell viability was determined using the WST-1 assay. Cells were seeded at a density of 6000 per well in a 96-well plate and cultured for 24 hours at 37 °C and 5% CO_2. The medium was then replaced with increasing concentrations (12.5, 25, 50, 100, 150, 200 μg mL^{-1}) of GMO@DTPA-BSA-Gd in DMEM, and the cells were incubated for an additional 24 hours under the same conditions. Then, the cells were washed three times with PBS, added with the fresh DMEM (200 μL) and 10 μL of Premix WST-1 reagent (Takara Bio Inc.) per well and incubated for 3 hours under the same conditions. Absorbance was measured at 450 nm, with 620 nm as a reference wavelength (Anthos Zenyth 340rt). The relative cell viability (%) was expressed as a percentage relative to the negative control (non-treated cells). Results were expressed as the mean of three replicates ± standard deviation.

2.3.3. Single cell inductively coupled plasma mass spectrometry (SC-ICP-MS) – cell uptake studies. For the studies of the efficiency of nanoparticles and resultant Gd^{3+} ion uptake by cells, cervical cancer cells (HeLa) were used. Cells were cultured in Dulbecco's modified Eagle's medium (DMEM, ThermoFisher Scientific) supplemented with 10% fetal bovine serum (FBS, Gibco Qualified, ThermoFisher Scientific) and 100 units per mL penicillin–streptomycin (ThermoFisher Scientific) and maintained under standard cell culture conditions at 37 °C in a humidified atmosphere containing 5% CO_2. Next, cells were incubated for 24 h with the prepared nanoparticle dispersions (50 μg mL^{-1} of lipid nanoparticles). Then, the medium containing nanoparticles was removed from the cell culture, and cells were washed several times with phosphate buffer solution (PBS, Merck) harvested using trypsin/EDTA (Merck) and fixed with 3.7% formaldehyde. Before the analysis, fixed cells were washed with PBS by centrifugation, and the obtained cell pellet was resuspended in PBS. For the SC-ICP-MS analysis, the exact cell concentration within the suspension was counted, and proper dilution (up to 100 000 cell per mL, set up requirements) was prepared. The analyses were performed on a NexION 5000 Multi-Quadrupole ICP-MS/MS (PerkinElmer) apparatus using a Single Cell (SC) application. The reference colloidal gold nanoparticles (30 nm, LGC Group) were used for transport efficiency determination. Analyses were performed in Standard mode, with Q3 only (Single Quad mode) scan, using the single cell spray chamber.

3. Results and discussion

The strategy for the preparation of an alternative biocompatible Gd-based contrast agent, presented in this study, relies on soft lipid nanoparticles, which have recently been increasingly and more often exploited as nanomedicine/nanocarrier with positive outcomes, also in clinical and even commercial use.[15] The lipid nanoparticles proposed here are nanoassemblies of high molecular weight amphiphile molecules of biocompatible GMO lipid, serving as a structure-forming matrix,[16,17] and DTPA-BSA-Gd a Gd-chelating lipid, as a source of paramagnetic metal.[9] Pluronic F127 was used as a common surfactant, providing steric stabilization to nanoparticles.[13] Samples after homogenization appear as stable milky-white colloidal dispersions for un-modified 2GMO-F127 (10, 15, 25% w/w F127) systems and milky but translucent for GMO-DTPA systems.

3.1. Morphology and structure of dispersions

As observed with cryo-TEM and supported by the FFT analysis, unmodified 2GMO-F127 (10, 15, 25% w/w F127) systems (Fig. 1A) and those modified with a low 5% w/w content of DTPA-BSA-Gd (2GMO-5DTPA) (Fig. 1B) constitute nanoparticles with a highly ordered, periodic internal structure, next to the populations of nanoparticles representing other forms of amphiphile self-assembled systems, such as liposomes, particularly in the case of nanoassemblies with the highest 25% w/w F127 content. SAXS analysis confirms these nanoassemblies' internal ordering, reflecting the *Pn3m* diamond bicontinuous cubic phase (Fig. 2A and Table S1, ESI†). In addition, the shift of peaks toward smaller values of the scattering vector q is observed for these systems, in comparison to unmodified 2GMO-25F127, most likely due to the more efficient structure's swelling facilitated by surfactants. The intensity of peaks decreases along with increasing surfactant content, which may be due to the decreasing number of nanoparticles exhibiting cubic phase compared to the increasing number of liposomes or micelles-like particles. Further, cryo-TEM analysis shows that systems with higher content of second amphiphile,

DTPA-BSA-Gd (30, 40, 50% w/w) (Fig. 1C), yielded nanoparticles with visibly disturbed structure. For the content of DTPA-BSA-Gd at 30% w/w, lipid nanoparticles were formed into a bistructural system consisting of relatively large vesicles with complex structures attached to their surface resolved from cryo-TEM pictures as a possible cubic one, mainly concluded based on SAXS data (Fig. 2B and Table S1, ESI†) for this system showing the existence of two different phases – lamellar and primitive cubic. A more detailed analysis of small-angle X-ray scattering (SAXS) revealed the presence of the dominant liposome fraction (attributed to the L_α phase) observed in cryo-TEM. Additionally, there are discernible reflections originating from the coexistence of a primitive cubic phase (*Im3m*) and a diamond cubic phase (*Pn3m*) present at very low contents. The intensity of peaks seems to elevate with higher DTPA-BSA-Gd content, particularly when contrasted with 2GMO-5DTPA-25F127. These results indicate that incorporating the DTPA-BSA-Gd lipid molecules into the GMO lipid bilayer at higher content disturbs the self-assembly of the lipid bilayer into more typical for GMO cubic *Pn3m* structure and rather induces transformation towards lamellar or even multilamellar phases also observed in cryo-TEM results (Fig. 1C). For the 30 and 40% w/w of DTPA-BSA-Gd content, the broad peak (Fig. 2B) denoted with a question mark was found on the scattering curve (q around 0.18 Å^{-1}) that cannot be simply assigned to any previously resolved phases. It was tentatively assumed that the origin of this peak was the lamellar structure of separate liposomes in the colloidal dispersion of lipid nanoparticles arising from DTPA-BSA-Gd chelates. A similar effect was presented in the work of Liu *et al.*,[18] wherein the studied Gd-oleate/Myverol (GMO) system, in the formed nanoparticles of the cubic phase, Gd-oleate was only partially incorporated in Myverol (GMO). At concentrations above 1% w/w, partial phase separation in the mentioned system occurred, with the formation of a lamellar phase rich in Gd-oleate, observed as the presence of a high liposome fraction next to the cubic one. In other studies, given by Gupta *et al.*[10] and Gupta *et al.*,[11] it is presented that the incorporation of Gd-chelating lipid into the lipid matrix, based not only on GMO but also on phytantriol (Gd-DTPA-MO-GMO and Gd-DTPA-monophytanyl-PT, respectively), a similar phase transition takes place.

3.2. Particle size, zeta potential, stability

The particle size parameters ($D_{\text{Intensity}}$, D_{Number}, Z-average, PdI) and the zeta potential of prepared unmodified nanoassemblies and those with incorporated DTPA-BSA-Gd are not affected by the compositional changes. The particle size remains within the range of roughly 160–190 nm (as for $D_{\text{Intensity}}$) and PdI below 0.25, indicating a medium-range of polydispersity characteristics of prepared nanoparticle dispersions. The average sizes of the prepared nanoassemblies are consistent with those observed in cryo-TEM images. The ζ remains negative for all dispersions and falls into the absolute value range of 7.5–18.5 mV, providing fair colloidal stability of the systems. The particle size parameters and ζ of all tested systems remain at similar values over the following weeks with small fluctuations. This confirms that they maintain colloidal stability, which is an added value in the case of drug delivery and other biomedical applications.[15] Furthermore, the results do not show an effect of the surfactant content on the particle size parameters and ζ. The summary of DLS and zeta potential results are reported in Table 1, whereas the long-term stability over 7 weeks of particle size parameters and ζ is given in Fig. 3 for 2GMO-25F127 and 2GMO-50DTPA-25F127 as representative samples. The results for all investigated nanoassemblies are given in Fig. S3–S6 (ESI†).

3.3. Gd^{3+} ion content analysis

Since the prepared nanoassemblies are expected to deliver Gd^{3+} ions efficiently to the MR imaged area of interest and exhibit reduced Gd-associated toxicity, they were analyzed towards the final molar concentration of Gd^{3+} ions in the prepared nanoparticle dispersions after mineralization ($[Gd^{3+}]_{\text{FinalSTD}}$)

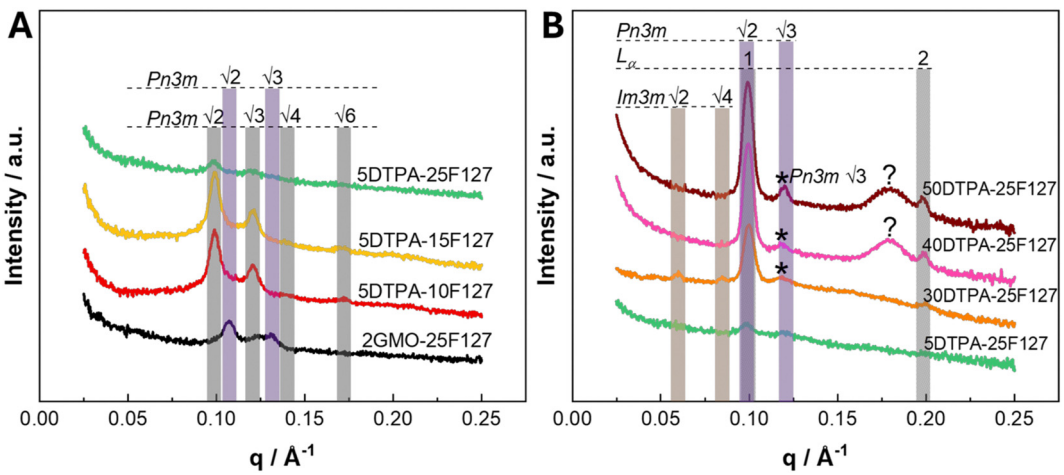

Fig. 2 SAXS scattering curves of (A) unmodified system (2GMO-25F127) along with nanoassemblies with low DTPA-BSA-Gd content (5% w/w), but with different concentrations of surfactant Pluronic F127 (10, 15, 25% w/w); (B) nanoassemblies with high DTPA-BSA-Gd content (30, 40, 50% w/w) and the same content of surfactant Pluronic F127 (25% w/w) compared to 2GMO-5DTPA-25F127.

Table 1 Summary of DLS results: particle size distribution ($D_{Intensity}$-intensity weighted distribution), polydispersity index (PdI), and zeta potential (ζ), including standard deviation (SD, n = 3). Measurements were performed at 22 °C after 24 hours of nanoparticle dispersion stabilization after the preparation

Sample	$D_{Intensity}$ ± SD/nm	PDI	ζ/mV
2GMO-10F127	176.6 ± 7.3	0.200 ± 0.017	−12.90 ± 0.10
2GMO-15F127	186.5 ± 0.9	0.220 ± 0.010	−18.40 ± 1.40
2GMO-25F127	168.4 ± 2.8	0.230 ± 0.011	−17.40 ± 0.47
2GMO-5DTPA-10F127	170.7 ± 8.2	0.172 ± 0.025	−6.46 ± 1.21
2GMO-5DTPA-15F127	173.9 ± 3.9	0.183 ± 0.004	−7.30 ± 0.60
2GMO-5DTPA-25F127	176.7 ± 4.5	0.198 ± 0.021	−16.30 ± 0.07
2GMO-40DTPA-10F127	158.7 ± 3.9	0.131 ± 0.033	−13.40 ± 1.56
2GMO-40DTPA-15F127	177.8 ± 5.1	0.216 ± 0.016	−9.43 ± 0.85
2GMO-40DTPA-25F127	177.9 ± 0.4	0.112 ± 0.005	−7.53 ± 0.47
2GMO-30DTPA-25F127	163.9 ± 6.9	0.146 ± 0.006	−7.96 ± 0.21
2GMO-50DTPA-25F127	161.8 ± 7.7	0.240 ± 0.010	−7.51 ± 0.26

(Table 2). Results are compared with the initial concentration of Gd^{3+} ions in the lipid mixture before the homogenization ($[Gd^{3+}]_{Initial}$). As expected, the $[Gd^{3+}]_{FinalSTD}$ is lower than $[Gd^{3+}]_{Initial}$. Standard ICP-MS analysis showed that the Gd^{3+} ion content in prepared samples with low (5% w/w) and high (30, 40, 50% w/w) DTPA-BSA-Gd lipid contents differs roughly by one order of magnitude. This is consistent with the initial concentration of lipid used for nanoassembly preparation. The calculated loading efficiency (LE) (Table 2) is high and reaches, *e.g.*, 85.3% for 2GMO-30DTPA-25F127, which indicates the effective incorporation of DTPA-BSA-Gd lipid into the GMO matrix. However, some exceptions are observed, *e.g.*, 34.0% for 2GMO-40DTPA-10F127 or 58.5% for 2GMO-50DTPA-25F127. LE, in general, increases with the increasing content of surfactant within the nanoassemblies with both 5% w/w and 40% w/w DTPA-BSA-Gd. In the set of nanoassemblies with increasing content of DTPA-BSA-Gd (30, 40, 50% w/w), LE decreases. This suggests that the incorporation of DTPA-BSA-Gd within the GMO matrix during nanoassembly formation is limited, and as discussed above, it has a significant impact on the structure and morphology of prepared nanoassemblies.

3.4. Biocompatibility *in vitro*

Firstly, the impact of increasing concentrations of surfactant Pluronic F127 on the cytotoxicity in HeLa and MSU 1.1 cells was evaluated (Fig. 4). As observed, there was no cytotoxic effect in HeLa cells up to 150 μg mL^{-1} in the three different DTPA-BSA-Gd content (30, 40, 50% w/w) nanoassembly dispersions. At 200 μg mL^{-1}, the viability for 2GMO-40DTPA-10F127 remained unchanged, while for 2GMO-40DTPA-15F127 and 2GMO-40DTPA-25F127, the viability dropped to about 30%. In MSU 1.1 cells, no cytotoxic effect was observed up to 100 μg mL^{-1}. At 150 μg mL^{-1} and 200 μg mL^{-1}, viability gradually decreased across all samples. In cells treated with 2GMO-40DTPA-10F127, viability decreased up to 80% at 200 μg mL^{-1}, while in those treated with 2GMO-40DTPA-15F127 and 2GMO-40DTPA-25F127, it was reduced to 40%. These results reflect the impact of the surfactant on the cytotoxicity of 2GMO-40DTPA nanoparticles and are consistent with previous reports.

Jagielski *et al.*[16] investigated the cytotoxicity of pure GMO lipid liquid crystalline nanoparticles (LLCNPs) on HeLa and MSU 1.1 cells, reporting a drop in viability for both cell lines at 100 μg mL^{-1}. Similarly, Hinton *et al.*[19] observed no cytotoxic effect on CHO cells below 100 μg mL^{-1} for GMO LLCNPs. On the other hand, Astofil *et al.*[20] reported no cytotoxic effect of GMO LLCNPs on STO cells up to 200 μg mL^{-1}. Generally, the lower cytotoxicity of prepared GMO-DTPA-F127 nanoassemblies might be attributed to the lipid composition, suggesting that a higher contribution of GMO leads to a greater cytotoxic effect. Although F127 is typically considered a non-toxic component of lipid nanoparticles, at sufficiently high concentrations, it can disrupt mammalian cell membranes.[21] Thus, F127 can exhibit actual cytotoxic effects, particularly at concentrations above 200 μg mL^{-1} in nanoassemblies with 25% w/w.

Further, the effect of DTPA-BSA-Gd, and consequently Gd, on cellular viability was assessed. No significant differences in cytotoxicity were observed for HeLa cells treated with 2GMO-30/40/50DTPA-25F127 at concentrations up to 150 μg mL^{-1}. Above that concentration, a decrease in viability to approximately 30% for cells treated with all-types nanoassemblies was observed. In contrast, MSU 1.1 cells demonstrated higher sensitivity to 2GMO-30/40/50DTPA-25F127 treatment. Up to 100 μg mL^{-1}, the viability of cells remained at approximately 100%, but above that concentration, it gradually decreased to around 40%.

These results suggest that GMO-DTPA-F127 nanoassemblies preserve high biocompatibility towards both cancer and normal cells, specifically, up to 150 μg mL^{-1} for HeLa cells and up to 100 μg mL^{-1} for MSU 1.1 cells. At higher nanoparticle concentrations (above 150/200 μg mL^{-1}), the surfactant content is a factor negatively affecting the viability profiles. These results align with the previously reported studies on the cytotoxicity of nanoassemblies with different types of gadolinium-DTPA amphiphiles.[22]

3.5. Up-take studies – Gd^{3+} ion content in single cells

The cell uptake of the prepared nanoassemblies containing Gd^{3+} ions was performed with the SC-ICP-MS technique, allowing for rapid and robust analysis of a large number of individual intact cells. Nanoassemblies with three different contents of DTPA-BSA-Gd were used for uptake studies, 2GMO-30DTPA-25F127, 2GMO-40DTPA-25F127, 2GMO-50DTPA-25F127, and compared to non-treated cells. Results indicate that the uptake of prepared nanoassemblies into model cancer HeLa cells is not homogenous in terms of the mass of Gd per cell since the distribution of uptake in the cell population was observed. The analysis also reveals the effect of nanoparticle composition, as the mean mass of Gd^{3+} per cell was 627.33 attogram (ag) for 2GMO-30DTPA-25F127, 995.67 ag for 2GMO-40DTPA-25F127 and 1386.67 ag for 2GMO-50DTPA-25F127 (Fig. 5). This must be accounted for when developing carriers for imaging agent since their efficiency is strongly related to their interaction with cells, sufficient delivery of Gd^{3+} ions, and their resultant diagnostic effects, here enhanced r_1 relaxivity. The above results of mean mass accounted for the measured dominant single

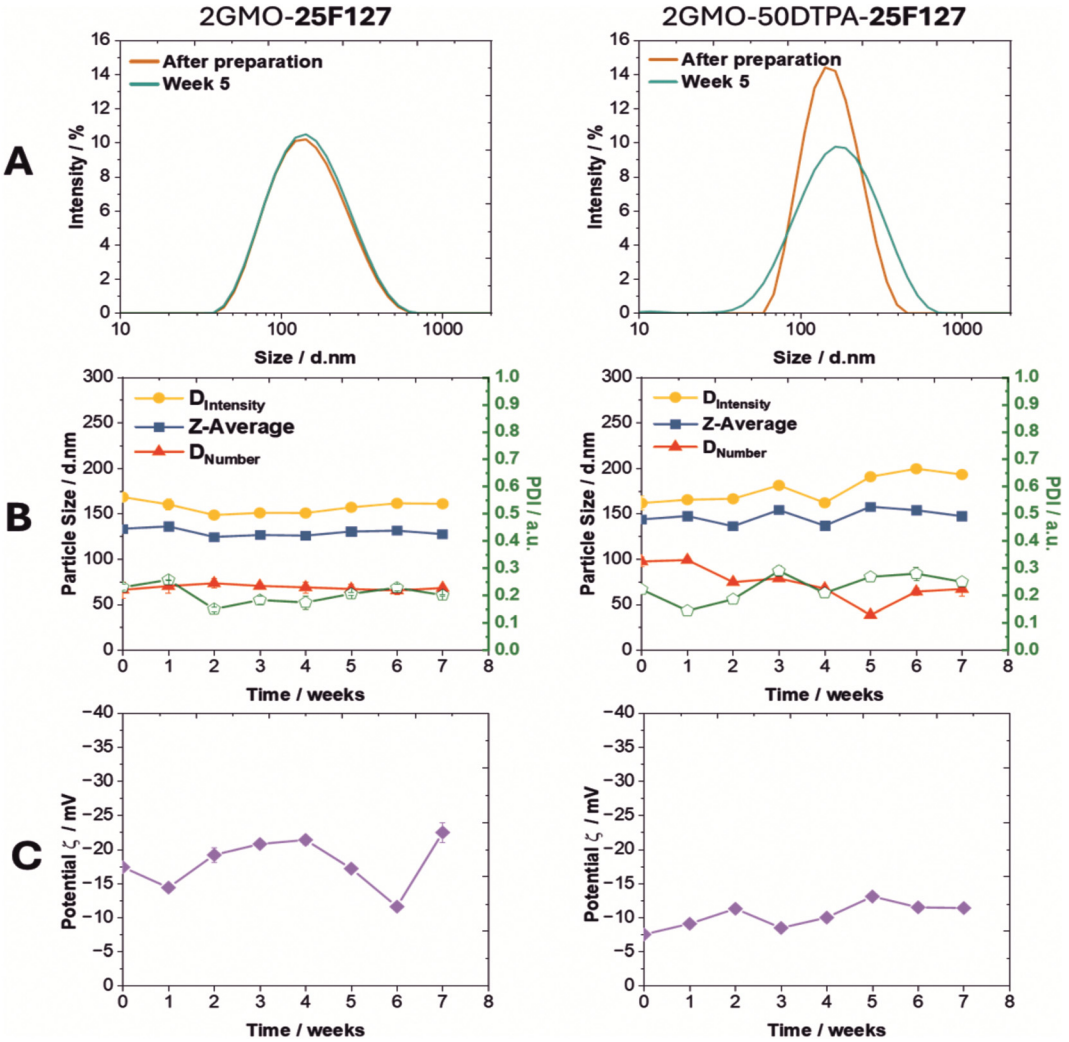

Fig. 3 Dynamic light scattering (DLS) results ((A) particle size distribution curves weighed by intensity for chosen time points (0 – after preparation and after 5 weeks), and (B) particle size weighed by intensity ($D_{Intensity}$), by number (D_{Number}), *Z*-average, polydispersity index (PDI), (C) potential ζ over 7 weeks for the un-modified system (2GMO-25F127) and nanoassemblies with 50% w/w of DTPA-BSA-Gd and 25% w/w of surfactant Pluronic F127 (2GMO-40DTPA-25F127).

cell fraction (80.75%, 76.15%, 68.27% for the following nanoassemblies) in terms of mean mass (range 1). The summary of results for all measured cell fraction ranges (range 1, 2, and 3) are given in Fig. S1 (ESI†), reflecting the mean mass per population of double cell agglomerates (range 2) and further numerous cell agglomerates (range 3). However, these fractions constitute approximately 20–30% of analyzed cells. Further, the analysis also revealed the contribution of ionic background at the nanomolar level (4.01, 7.65, 11.76 × 10^{-9} mol L^{-1}, respectively, for the following samples GMO-30DTPA-25F127, GMO-40DTPA-25F127, GMO-50DTPA-25F127), which suggests that nanoassemblies upon cell uptake undergo a certain intracellular metabolism (before cell fixation), leading to the disassembly of lipid nanoparticles and Gd^{3+} release from cell compartments and further outside the cell. In addition, lipid nanoparticles may interfere with the cell membrane and affect its permeability to uptaken ions outside.[23,24] As suggested by Reese *et al.*,[25] the NPs-cell contact could influence the dissolution of nanoparticles, and thus, additional ionic release at the particle–cell interface.

3.6. Relaxivity studies

Though the molar concentration in the prepared nanoparticle dispersions is not meaningfully different, the samples show a consequent difference in the relaxivity (r_1). The higher the molar concentration of Gd^{3+} in prepared particle dispersions, the shorter the longitudinal relaxation time (T_1). Using the measured T_1, the longitudinal relaxation rates (R_1) were calculated as $1/T_1$ and plotted as a function of Gd^{3+} ion concentration. Finally, the longitudinal relaxivity (r_1) was determined as a slope of the plotted dependence R_1 *vs.* [Gd^{3+}] ion concentration, using the equation: $R_1 = r_1*[Gd^{3+}] + 1/T_{1\_water}$. The summary of the obtained relaxivity parameters is given in Table 3. The R_1 *vs.* [Gd^{3+}] plots are presented in Fig. 6I, showing

Table 2 Gd^{3+} ion concentration of prepared nanoassemblies of different compositions: $[Gd^{3+}]_{Initial}$-initial molar concentration of Gd^{3+} ions in the lipid mixture before the homogenization; $[Gd^{3+}]_{FinalSTD}$-final molar concentration of Gd^{3+} ions in the prepared nanoparticle dispersions after mineralization determined with the standard ICP-MS; Gd^{3+} ion loading efficiency (LE)

Sample names	$[Gd^{3+}]_{Initial}$ (mM)	$[Gd^{3+}]_{FinalSTD}$ (mM)/RSD (%)	Gd^{3+} LE (%)/SD
2GMO-5DTPA-10F127	0.95	0.71/0.81	74.3/0.60
2GMO-5DTPA-15F127	0.95	0.75/0.67	78.9/0.53
2GMO-5DTPA-25F127	0.95	0.78/0.58	82.5/0.48
2GMO-40DTPA-10F127	7.60	2.59/0.33	34.0/0.11
2GMO-40DTPA-15F127	7.60	5.58/0.28	73.4/0.20
2GMO-40DTPA-25F127	7.60	6.12/0.16	80.6/0.13
2GMO-30DTPA-25F127	5.70	4.86/1.48	85.3/1.24
2GMO-50DTPA-25F127	9.50	5.56/0.24	58.5/0.14

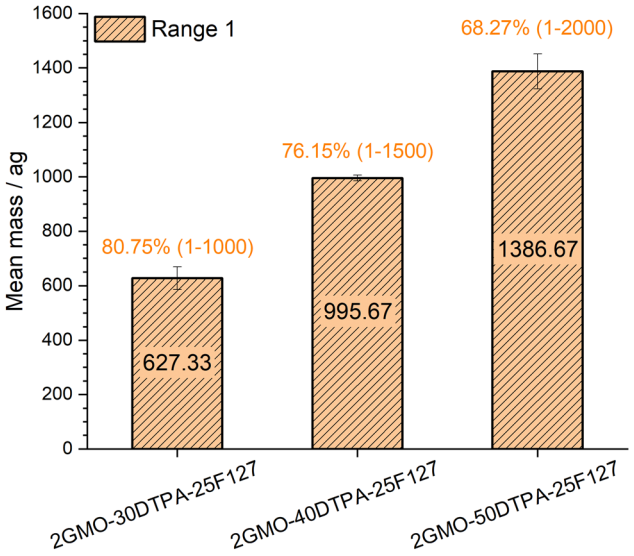

Fig. 5 Single cell inductively coupled plasma mass spectrometry ((SP)-ICP-MS)) uptake studies on HeLa cells treated with nanoassemblies of three different DTPA-BSA-Gd contents (30, 40, 50% w/w) and 25% w/w of surfactant Pluronic F127. Results show the mean mass of Gd per cell (expressed in attogram (ag)), accounted for the measured dominant single cell in terms of mean mass (range 1, insert in the figure).

the effect of the surfactant concentration (10, 15, 25% w/w) in prepared nanoassemblies with low 5% w/w (Fig. 6I-A) and high 40% w/w contents of DTPA-BSA-Gd (Fig. 6I-C), and the effect of initial Gd-chelating lipid concentration (30, 40, 50% w/w) at the same surfactant content (25% w/w) (Fig. 6I-B). The results reveal the effect of the surfactant content on r_1, as it decreases along with the increasing content of surfactant in the case of nanoassemblies with low 5% w/w content of DTPA-BSA-Gd, and also high content-exemplary 40% w/w DTPA-BSA-Gd. The comparison of r_1 for nanoassemblies with 30, 40, 50% w/w DTPA-BSA shows that r_1 also increases.

Since the Gd^{3+} ion concentration (Table 2, $[Gd^{3+}]_{FinalSTD}$) in the third set of nanoassemblies with 40% w/w DTPA-BSA-Gd significantly increases along with the increasing surfactant content, such lack of consequence between Gd^{3+} ion concentration and relaxivity is not clear. However, it could be explained that during the self-assembly, DTPA-BSA-Gd molecules cannot

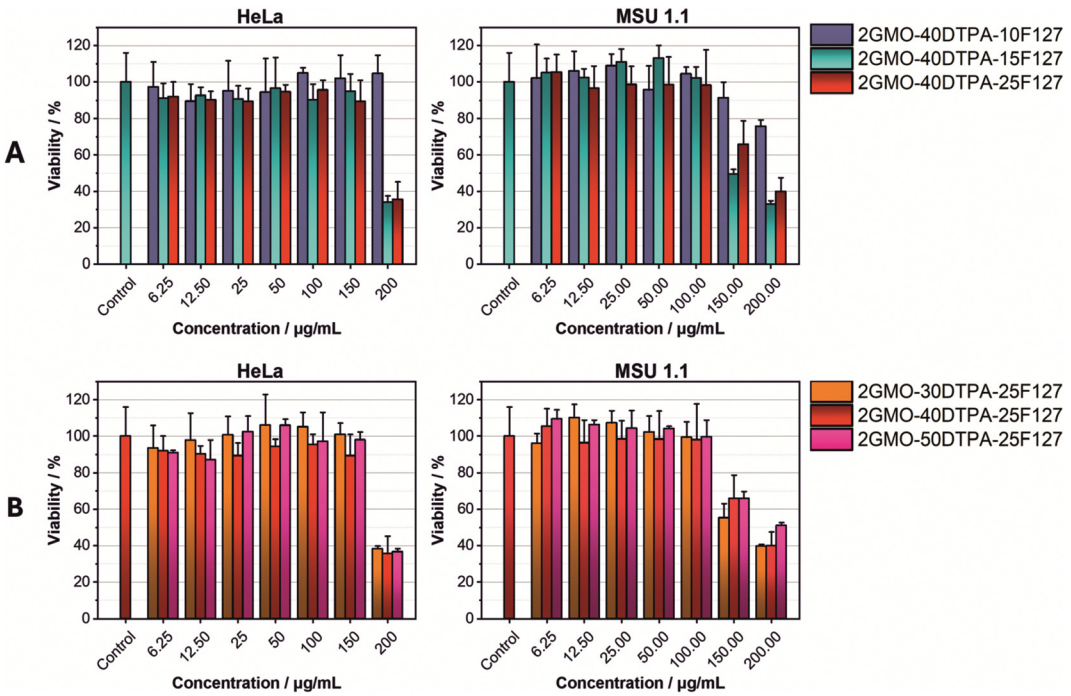

Fig. 4 Cell viability profiles of HeLa and MSU 1.1 cells treated with prepared nanoassemblies at different concentrations: (A) effect of surfactant-nanoassemblies with 40% w/w of DTPA-BSA-Gd and 10, 15 and 25% w/w of surfactant Pluronic F127; (B) effect of DTPA-BSA-Gd content – nanoassemblies with 30, 40, 50% w/w and with 25% w/w of surfactant Pluronic F127.

Table 3 Longitudinal relaxivity parameters (T_1-relaxation time; r_1-relaxivity) of prepared nanoassemblies of different compositions measured by NMR at a magnetic field of 0.39 T (16.5 MHz) at room temperature (23 °C). r_1 results are compared to other Gd-based MRI contrast agents (Magnevist, Gadovist, Dotarem, measured at 0.47 T, room temperature) and to similar lipid-based systems reported in the literature (Gd-DTPA-MP in PT, Gd-DTPA-MO in GMO measured at 0.54 T, room temperature)

Sample names	r_1/mM^{-1} s^{-1}
2GMO-5DTPA-10F127	8.50
2GMO-5DTPA-15F127	8.22
2GMO-5DTPA-25F127	5.15
2GMO-40DTPA-10F127	19.72
2GMO-40DTPA-15F127	11.56
2GMO-40DTPA-25F127	10.88
2GMO-30DTPA-25F127	8.87
2GMO-50DTPA-25F127	12.01
Magnevist[1]	3.4
Gadovist[1]	3.7
Dotarem[1]	3.4

be evenly distributed in the formed lipid bilayer, and the imbalance between Gd^{3+} ions facing inward and outward the formed nanoparticles may take place. Therefore, in this set of nanoassemblies, possibly more Gd^{3+} ions are facing inward, where they are screened from the interaction with water molecules for proton exchange. Surfactant molecules may additionally compete with the DTPA-BSA-Gd molecules during the self-assembly, negatively affecting their incorporation into the lipid bilayer, and finally, the internal ordering of nanoparticles. A similar effect was observed for lipid systems Gd-DTPA-BSA loaded into porphysomes composed of cholesterol, different phospholipids and pyrolipids (with modified stoichiometric compositions), where although high-density incorporation of Gd^{3+} ions was achieved, the relaxivity was less enhanced when compared to the system prepared with DTPA-Gd with a single alkyl chain.[9]

Nevertheless, the investigated nanoassemblies exhibit expected improved r_1 values (Table 3). The highest value of the most interesting relaxivity parameter r_1, 19.72 mM^{-1} s^{-1}, was achieved for 2GMO-40DTPA-10F127. The obtained r_1 parameters in this work of all studied nanoassemblies outperform those reported for Gd-based commercially developed contrast agents, such as Magnevist, Gadovist, or Dotarem, tested using a similar magnetic field of 0.47 T in water-based solutions at room temperature.[26] Similar results were presented in the work of Gupta *et al.*,[11] where at a similar magnetic field strength of 0.54 T, in the studied system of Gd-chelating lipids (Gd-DTPA-Monophytanyl) incorporated into the phytantriol matrix (PT), significantly higher values of r_1 were observed compared to the commercial contrast agent – Magnevist (r_1 = 3.4 mM^{-1} s^{-1}, 0.47 T[26]). Also, in another work by Gupta *et al.*[11] in a system based on a gadolinium-chelating lipid with an oleyl chain (Gd-DTPA-MO) in a GMO matrix, the r_1 was reported to be higher than that of Magnevist.

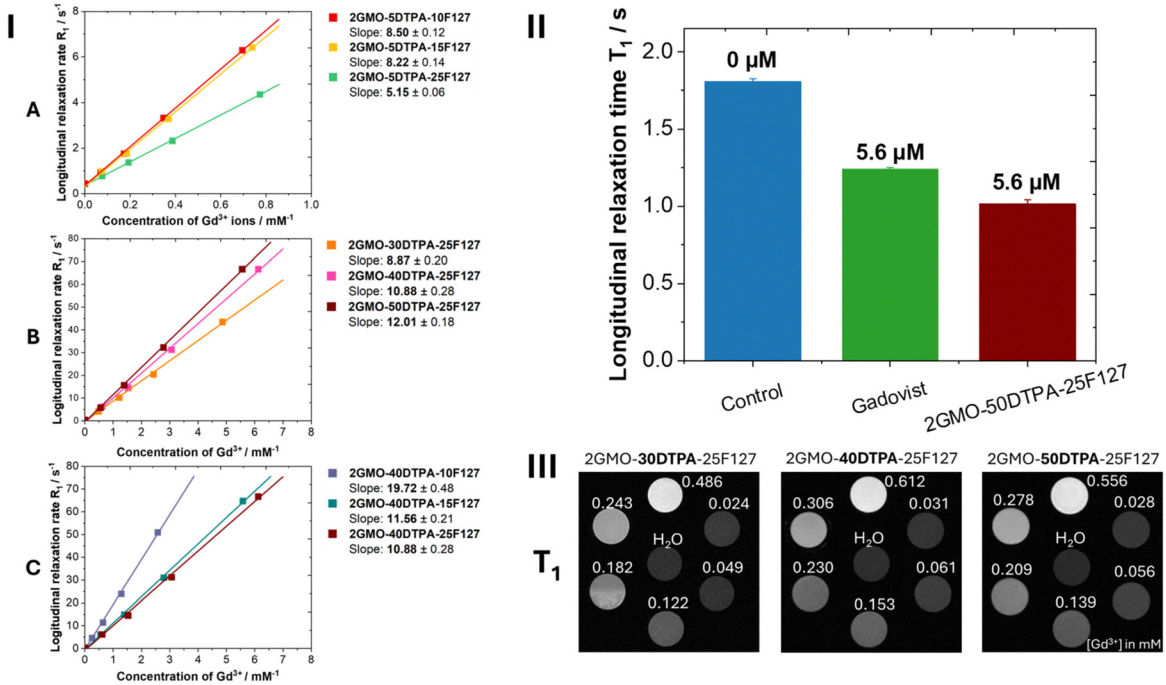

Fig. 6 (I) Dependence of the longitudinal relaxation rate R_1 on the concentration of Gd^{3+} ions for prepared nanoparticle dispersions: (A) nanoassemblies with low DTPA-BSA-Gd content (5% w/w) and with different concentrations of surfactant Pluronic F127 (10, 15, 25% w/w); (B) nanoassemblies with high DTPA-BSA-Gd contents (30, 40, 50% w/w) and the same content of surfactant Pluronic F127 (25% w/w); (C) nanoassemblies with 40% w/w DTPA-BSA-Gd and with different concentrations of surfactant Pluronic F127 (10, 15, 25% w/w). (II) Comparison of the longitudinal relaxation time (T_1) for non-treated (control) and cervical cancer cells (HeLa) treated with 2GMO-50DTPA-25F127 nanoassemblies and Gadovist (5.6 μM of Gd^{3+}). (III) T_1-weighted MR images of prepared nanoassemblies with high DTPA-BSA-Gd content (30, 40 and 50% w/w) and with 25% w/w of surfactant Pluronic F127 at different Gd^{3+} ion concentrations ([Gd^{3+}] in mM), collected with a 9.4 T MRI horizontal scanner at room temperature.

Finally, the applicability of prepared nanoassemblies (2GMO-50DTPA-25F127 as representative) as a potential MRI CA was assessed with the NMR studies performed on cervical cancer cells (HeLa). Results (Fig. 6II) show that 2GMO-50DTPA-25F127 shows lower longitudinal relaxation time (T_1 = 1.043 s) *vs.* Gadovist (T_1 = 1.241 s) at the same Gd concentration in the probe.

To sum up, the results of relaxation parameters obtained in this work for the prepared high molecular weight nanoassemblies of GMO@DTPA-BSA-Gd show the superiority over commercially developed low molecular weight and non-assembled contrast agents such as Magnevist, Gadovist, or Dotarem. This can be credited to their larger molecular weight and size, which result in a decreased tumbling rate, and thus, longer reorientation correlation times.[27] Moreover, tested self-assembling lipid systems may enable more efficient water proton exchange, resulting in higher relaxation for these systems, with some restrictions regarding the surfactant content in the system. The nanoassemblies in this work are based on two types of amphiphile molecules that offer a fair loading of coordinated Gd^{3+} ions and enable efficient water proton exchange between the inner and outer spheres surrounding the Gd^{3+} ions, finally resulting in better relaxation. An interesting conclusion is also that the prepared nanoassemblies with a higher content of Gd-chelating lipid (30, 40, 50% w/w) are characterized by a lower degree of internal order, and yet they show better parameters of longitudinal relaxation. Similar conclusions were presented by Moghaddam *et al.*[22] for Gd-DTPA nanoassemblies with different complexing amphiphiles, *i.e.*, with the mono- and bis-oleyl (Gd-DTPA-MO, Gd-DTPA-BO) and with mono- and bis-phytanyl (Gd-DTPA-MP, Gd-DTAP-BP). Likewise, the results in our previous work on hybrids of lipid liquid crystalline nanoparticles with MnO demonstrated such behavior of internal ordering *vs.* relaxivity.[17] However, to fully understand the impact of the various structures obtained on the relaxivity of the studied systems, it is necessary to determine the hydration state of Gd^{3+} and the correlation times from relaxometry and ^{17}O measurements, which is a challenge in the case of Gd^{3+}.[28]

3.7. MR imaging

To assess the efficiency of prepared nanoassemblies as MRI contrast agents, direct observations of the contrast enhancement in MR imaging using the prepared solutions of nanoparticle dispersions were performed. T_1-weighted MRI images (Fig. 6III) confirmed the effectiveness of prepared nanoparticle dispersions GMO-DTPA-F127 as T_1 positive contrast agents, owing to their high relaxivities (Table 3). As the molar concentration of Gd^{3+} increased, the brightening of the images was observed, indicating a clear relaxivity signal dependency on Gd ion concentration. Even though the paramagnetic Gd-based contrast agents are mainly used to brighten the image due to the shortening of T_1, the effectiveness of the prepared nanoparticle dispersions as T_2 negative contrast agents was also tested for comparison purposes (Fig. S2 in ESI†). T_2-weighted MRI images become increasingly darker as the concentration of Gd ion increases. However, the observed contrast changes in T_2-weighted images are not as efficient as in the case of T_1-weighted MRI images.

The results confirm the potential of prepared nanoassemblies as positive MRI contrast agents; however, further studies are necessary to improve the payload of Gd^{3+} ions into the GMO amphiphile matrix, including increased payload per nanoassembly and to understand the effect of the formed type of nanostructure on the relaxivity. Future work will also address the *in vivo* contrast enhancement and bio-distribution to unequivocally determine their final efficiency as positive MRI contrast agents.

4. Conclusions

This study presents the preparation of nanoassemblies using two types of amphiphiles, GMO as a matrix and Gd-chelating lipid DTPA-BSA-Gd as a paramagnetic ion source, stabilized with the surfactant Pluronic F127 molecules. As-prepared nanoassemblies are considered high molecular weight Gd ion-containing contrast agents for MR imaging. However, the preparation of such nanoassemblies has some limitations, as reported in this study. Structural analysis showed that in an environment rich in DTPA-BSA-Gd molecules (high DTPA-BSA-Gd content), next to the GMO molecules, the process of self-assembly into more curved cubic structures is disturbed. Instead, a lower degree of internal order or simply order of other type is observed within the formed nanoparticles. The prepared nanoparticles are stable in size and surface charge, including long-term observations. The proposed nanoassemblies are characterized by the high loading efficiency of Gd^{3+} ions, which confirms their strong entrapment within nanoparticles. The achieved final Gd^{3+} ion content (nanoassemblies with high 30, 40, 50% w/w of DTPA-BSA-Gd) translated into an improved high relaxivity r_1, which may compete with the one reported for Gd-based commercially developed contrast agents or other lipid-based nanoassemblies under similar measurement conditions reported in the literature. The study also showed that the surfactant content impacts the loading efficiency of DTPA-BSA-Gd within the GMO matrix upon nanoassembly formation, resulting in the increased content of Gd^{3+} ions. However, it is not further reflected accordingly in the obtained r_1 parameters. This was assigned to the inhomogeneous distribution of Gd^{3+} ions within the formed bilayer and then interior nanoassemblies, hampering an efficient water proton exchange. The comprehensive analysis also points out that a lower degree of internal ordering does not exclude the formed nanoassemblies as efficient MRI positive contrast enhancers, which was proven in the presented *in vitro* MRI results, where the contrast in the collected T_1-weighted images was brightened. The prepared nanoassemblies are also efficiently up-taken by cells, which was reflected in the Gd^{3+} ion content within the analyzed single cells, as well as in the T_1 NMR measurements in cell suspensions. Further, biocompatibility studies showed the proposed nanoassemblies are not toxic at the applied broad concentration range of nanoparticles,

and hence the metal-associated toxicity is not the case for this system, but the content of surfactant may play a negative role, particularly at higher nanoparticle concentrations. In summary, the lipid-based nanoassemblies proposed in the study can serve as a new type of high molecular weight contrast agent for MRI.

Author contributions

Karolina Dydak: conceptualization, investigation, formal analysis, visualization, methodology, and writing – original draft, review and editing; Tomasz Zalewski: conceptualization, investigation, formal analysis, visualization, methodology, and writing – review and editing; Marek Kempka: conceptualization, investigation, methodology, writing – review and editing; Patryk Florczak: conceptualization, investigation, formal analysis, methodology, writing – review and editing; Grzegorz Nowaczyk: conceptualization, resources, investigation, formal analysis, visualization, writing – original draft, review and editing, project administration, and funding acquisition; Łucja Przysiecka: conceptualization, investigation, methodology, writing – review and editing; Jakub Jagielski: conceptualization, investigation, methodology, writing – original draft, review and editing; Benoit Loppinet: conceptualization, investigation, methodology, writing – review and editing; Michał Banaszak: conceptualization, resources, writing – review and editing; Dorota Flak: conceptualization, investigation, formal analysis, visualization, writing – original draft, review and editing.

Data availability

The data supporting this article have been included as part of the ESI.†

Conflicts of interest

The authors declare no competing interests.

Acknowledgements

The work was financially supported by the research grant Sonata Bis 2016/22/E/ST3/00458 from the National Science Centre, Poland. The SAXS measurements were performed under the support of the Hellenic Foundation for Research and Technology (H.F.R.I.) under the ''1st Call for H.F.R.I. Research Projects to support Faculty Members and Researchers and the Procurement of high-cost research equipment grant'' (Project Number: HFRI-FM17C3-3401, SAXS-SOFT).''

Notes and references

1 J. Wallyn, N. Anton, S. Akram and T. F. Vandamme, *Pharm. Res.*, 2019, **36**, 78.
2 H.-J. Weinmann, R. C. Brasch, W.-R. Press, G. E. Wesbey and J. Weinmann, *Am. J. Roentgenol.*, 1984, **142**, 619–624.
3 J. Wahsner, E. M. Gale, A. Rodríguez-Rodríguez and P. Caravan, *Chem. Rev.*, 2019, **119**, 957–1057.
4 Y. D. Xiao, R. Paudel, J. Liu, C. Ma, Z. S. Zhang and S. K. Zhou, *Int. J. Mol. Med.*, 2016, **38**, 1319–1326.
5 Z. Zhou and Z. R. Lu, *Wiley Interdiscip. Rev.: Nanomed. Nanobiotechnol.*, 2013, **5**, 1–18.
6 M. Jeon, M. V. Halbert, Z. R. Stephen and M. Zhang, *Adv. Mat.*, 2021, **33**, 1906539.
7 J. J. Yang, J. Yang, L. Wei, O. Zurkiya, W. Yang, S. Li, J. Zou, Y. Zhou, A. L. W. Maniccia, H. Mao, F. Zhao, R. Malchow, S. Zhao, J. Johnson, X. Hu, E. Krogstad and Z.-R. Liu, *J. Am. Chem. Soc.*, 2008, **130**, 9260–9267.
8 P. Mi, H. Cabral, D. Kokuryo, M. Rafi, Y. Terada, I. Aoki, T. Saga, I. Takehiko, N. Nishiyama and K. Kataoka, *Biomaterials*, 2013, **34**, 492–500.
9 D. A. Margalik, J. Chen, T. Ho, L. Ding, A. Dhaliwal, A. S. Doria and G. Zheng, *Bioconjugate Chem.*, 2022, **33**, 2213–2222.
10 A. Gupta, T. Stait-Gardner, L. De Campo, L. J. Waddington, N. Kirby, W. S. Price and M. J. Moghaddam, *J. Mater. Chem. B*, 2014, **2**, 1225–1233.
11 A. Gupta, L. De Campo, B. Rehmanjan, S. A. Willis, L. J. Waddington, T. Stait-Gardner, N. Kirby, W. S. Price and M. J. Moghaddam, *Langmuir*, 2015, **31**, 1556–1563.
12 D. K. Flak, V. Adamski, G. Nowaczyk, K. Szutkowski, M. Synowitz, S. Jurga and J. Held-Feindt, *Int. J. Nanomed.*, 2020, **15**, 7415–7431.
13 S. P. Akhlaghi, I. R. Ribeiro, B. J. Boyd and W. Loh, *Colloids Surf., B*, 2016, **145**, 845–853.
14 X. Wei, M. Ying, D. Dehaini, Y. Su, A. V. Kroll, J. Zhou, W. Gao, R. H. Fang, S. Chien and L. Zhang, *ACS Nano*, 2018, **12**, 109–116.
15 L. Xu, X. Wang, Y. Liu, G. Yang, R. J. Falconer and C. X. Zhao, *Adv. Nanobiomed. Res.*, 2022, **2**, 2100109.
16 J. Jagielski, Ł. Przysiecka, D. Flak, M. Diak, Z. Pietralik-Molińska, M. Kozak, S. Jurga and G. Nowaczyk, *J. Nanobiotechnol.*, 2021, **19**, 168.
17 D. Flak, T. Zalewski, K. Fiedorowicz, Ł. Przysiecka, M. Jarek, A. Klimaszyk, M. Kempka, A. Zimna, N. Rozwadowska, J. Avaro, M. Liebi and G. Nowaczyk, *J. Mater. Chem. B*, 2023, **11**, 8732–8753.
18 G. Liu, C. E. Conn, L. J. Waddington, S. T. Mudie and C. J. Drummond, *Langmuir*, 2010, **26**, 2383–2391.
19 T. M. Hinton, F. Grusche, D. Acharya, R. Shukla, V. Bansal, L. J. Waddington, P. Monaghan and B. W. Muir, *Toxicol. Res.*, 2014, **3**, 11–22.
20 P. Astolfi, E. Giorgini, V. Gambini, B. Rossi, L. Vaccari, F. Vita, O. Francescangeli, C. Marchini and M. Pisani, *Langmuir*, 2017, **33**, 12369–12378.
21 S. F. Kahattak, S. R. Bhatia and S. C. Roberts, *Tissue Eng.*, 2005, **11**, 975–983.
22 M. J. Moghaddam, L. De Campo, M. Hirabayashi, P. A. Bean, L. J. Waddington, J. A. Scoble, G. Coia and C. J. Drummond, *Biomater. Sci.*, 2014, **2**, 924–935.

23 E. Di Gregorio, E. Gianolio, R. Stefania, G. Barutello, G. Digilio and S. Aime, *Anal. Chem.*, 2013, **85**, 5627–5631.
24 R. Zhang, X. Qin, F. Kong, P. Chen and G. Pan, *Drug Delivery*, 2019, **26**, 328–342.
25 P. Rees, J. W. Wills, M. R. Brown, C. M. Barnes and H. D. Summers, *Nat. Commun.*, 2019, **10**, 2341.
26 M. Rohrer, H. Bauer, J. Mintorovitch, M. Requardt and H.-J. Weinmann, *Invest. Radiol.*, 2005, **40**, 715–724.
27 M. A. Bruckman, X. Yu and N. F. Steinmetz, *Nanotechnology*, 2013, **24**, 462001.
28 R. Zairov, G. Khakimullina, S. Podyachev, I. Nizameev, G. Safiullin, R. Amirov, A. Vomiero and A. Mustafina, *Sci. Rep.*, 2017, **7**, 14010.